Journal of Sound and Vibration 326 (2009) 456–475

Contents lists available at ScienceDirect

Journal of Sound and Vibration

journal homepage: www.elsevier.com/locate/jsvi

A generalized approach for active control of structural-interior global noise

Simon G. Hill [a,*], Nobuo Tanaka [a], Scott D. Snyder [b]

[a] Department of Aerospace Engineering, Tokyo Metropolitan University, 6-6 Asahigaoka, Hino-shi, Tokyo 191-0065, Japan
[b] Corporate Services, Charles Darwin University, Darwin, Northern Territory 0909, Australia

ARTICLE INFO

Article history:
Received 15 January 2009
Received in revised form
16 June 2009
Accepted 16 June 2009
Handling Editor: C.L. Morfey

ABSTRACT

A generalized approach to the sensing of orthogonal functions, to the global error (potential energy) for a source radiating into an enclosure is presented. The developed orthogonal functions are generalized, as they are fundamentally acoustic based and thus not constrained to being structural or written in terms of structural measurements. Therefore application can be made to *any* noise source, facilitating wide practical implementation of the technique. The presented acoustic-centric technique for the sensing and control of enclosure noise, by being based on the fundamental acoustic radiation shape—the monopole, thus overcoming the need for any information of the noise source (other than its approximate size) in the construction of orthogonal functions contributing to the noise within the enclosure. The presented approach then makes a significant improvement over previous work in the area of orthogonal developments for radiation into enclosures, which has typically taken a vibration-centric approach postulating vibration domain measurements to construct the global performance criterion. Therefore providing the hope of moving beyond small-scale laboratory implementations to more practical problems. Simulations are completed to illustrate the validity of the novel approach by illustrating that a controller minimizing the generalized orthogonal functions will achieve the maximum possible attenuation of the global error.

1. Introduction

The situation where a noise source radiates into an enclosure and causes unwanted noise disturbance is common in many industries, for example the aerospace, aviation, automotive and marine industries. In most cases the problem is caused by some structural excitation resulting in a coupled vibro-acoustic enclosure. As these radiation problems within cavities are typically structure-borne noise, the problem has generally been tackled from a 'structural' point of view (i.e. using structural sensors and structural control sources). Such an approach has lead to active control developments being solely based on vibration characteristics of the radiating structure. In turn the sensing and control of sound transmission has become dependent on the structure itself (vibration characteristics), rather than the acoustic nature of the sound radiation. The reliance on a structural-centric approach to structural–cavity problems has limited applications to small-scale laboratory implementations.

* Corresponding author.
E-mail addresses: sghill@sd.tmu.ac.jp (S.G. Hill), ntanaka@cc.tmit.ac.jp (N. Tanaka), scott.snyder@cdu.edu.au (S.D. Snyder).

0022-460X/$ - see front matter © 2009 Elsevier Ltd. All rights reserved.
doi:10.1016/j.jsv.2009.06.014

In the area of active control of cavity noise, the literature concentrates on structural transmission into the cavity. Early work sought to quantify the mechanisms of sound transmission in closed shells and the modal coupling between structural vibration and the acoustic fields in such situations [1–5]. Early theoretical work aimed at achieving global reductions through active control showed that attenuation within cavities can be achieved using acoustic point sources [6,7]. The early practical active noise control systems, targeted noise within cylinders and the work established that structural point forces could control locally [8] and globally (through the minimization of the cavity acoustic modes) [9–11] noise within the cavity. For the active control community, the most common target structure for structural–cavity noise has been a rectangular enclosure with one flexible surface [12–19]. The general methodology required to examine the active control of this system arrangement and the several mechanisms which achieve global attenuation of the cavity noise can be found in the literature [13,15,16].

Pan et al. showed theoretically [12] and experimentally [13] that there are two different control mechanisms involved in the point force (structural control) minimization of sound transmission through a panel into an enclosure. If the system response is dominated by panel controlled modes, minimum sound energy is obtained by suppressing the panel vibration. If the system response is dominated by cavity controlled modes the control force is used to adjust the panel velocity distribution so that the real part of the power radiated from the panel into the cavity is minimized. In the latter case there may be an increased locally reactive intensity flow and increased vibration levels. The fundamental mechanics of active control of structural–cavity problems are further expanded on in a vibration mode-centric analysis in the literature [15,16].

A problem of a vibration mode approach is that as the system complexity increases more and more structural modes are required to be controlled. To overcome this problem 'transformed modes', or 'power modes', have been proposed where weighted combinations of structural modes (which form orthogonal shapes to the sound transmission from the panel into the cavity) are the error signals to be minimized [14]. Similar shapes were developed for a cylindrical cavity with a rectangular floor [20]. In these developments the number of orthogonal patterns that need to be controlled to reduce cavity noise is much less than the number of vibration modes to measure and control over the same frequency range. As less control channels are required the result is simpler and more robust active system. More recently, a new method where clusters of the structural–acoustic modes are formed based on the indices of the structural and acoustic cavity modes have been proposed in an attempt to simplify implementation [18,19]. However, all of these systems are built on the fundamental premise that structural information is available, which seems to have limited application to the laboratory.

What is sought here is a generalized decomposition of noise radiating into an enclosure, which can be applied to *any* noise source. In other words; a method where a bunch of sensors could be included on/within an enclosure along with a small number of control actuators, and then the active control system simply turned on. To achieve this several aspects of the design need to be constrained. Firstly the noise radiation transmission to the cavity needs to be classified into a set of *generalized acoustic functions*, removing the need for structural information. The goal of the sensing system is then to measure sound transmission via measuring the *generalized acoustic functions*. Attenuation can then be achieved, through a variety of methods, by minimizing these generalized functions.

In this work a set of acoustic functions are used to decompose radiation from any source, that is a set of acoustic functions (defined here as acoustic multipoles) are imposed onto the noise source. The end result in the decomposition process is a set of acoustic functions that are orthogonal to the global error. In the past elemental radiators have been applied to free field structural radiation, in an attempt to generalize the set of orthogonal vibration patterns to sound power [21]. The orthogonal shapes in this case are combinations of the elemental radiator amplitudes defined by the eigenvectors of the radiation transfer matrix. It is important to note that these vibration patterns are orthogonal to *sound power*, a different global error criterion to the global error in a cavity; and there is no reason to first constrain the analysis here to the decomposition of sound power and then use these shapes for acoustic potential energy.

Rather than looking at the problem from a structural point of view, an acoustic approach is taken, as illustrated in Fig. 1. More specifically the global error will be defined in terms of a set of sound pressure measurements, *not* structural measurements. The work here then provides a new way of looking at the structural–cavity problem; and as a result of being acoustic-centric provides a more direct, and thus precise, measure and method to control the acoustic global error within a

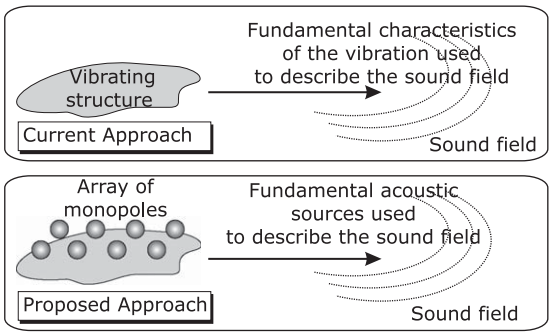

Fig. 1. The proposed novel approach to active control within cavities contrasted by the current approach.

cavity. Essentially the goal is to treat all situations the same, and so in a practical implementation the designer simply installs a number of sensors and actuators, immediately turns on the sensing and control technique, eliminating the lengthy system characterization that is necessary in approaches which require structural characteristics (for example structural mode shapes). The presented generalized methodology uses acoustic radiation shapes built on the fundamental radiation pattern of a monopole. The work is similar to the approach presented in theory and practice for global control in acoustic free field of two- and three-dimensional noise sources [22–27]. Finally simulations are presented to validate the presented theoretical approach.

2. Global performance development

Where a noise source is creating an annoyance and/or causing hearing damage, the ideal solution is one where the noise is globally attenuated. A global cost function will be developed as only this error will maximize the area and the number of people who can be positively influenced by an active control system. Consider a generic noise source radiating noise into an enclosure, the aim of a practical active control system is to measure and minimize a set of states that will lead to a reduction in a global error. The global cost function, J, is conveniently written as a quadratic function

$$J = \mathbf{q}^{\mathrm{T}}\mathbf{A}\mathbf{q} \tag{1}$$

In Eq. (1), $\mathbf{q}$ is a vector of quantities to be measured (essentially system states) and $\mathbf{A}$ is a square weighting matrix which defines the contribution of the states to the global error. If $\mathbf{A}$ is diagonal, each state in $\mathbf{q}$ contributes independently to the global performance measure J and a reduction in the global error is achieved by simply minimizing the states in $\mathbf{q}$. If $\mathbf{A}$ is not diagonal, the diagonal terms define the contribution to the global error of each element in $\mathbf{q}$ acting alone; the off diagonal terms define the modification of the isolated states in $\mathbf{q}$ due to the presence of the other states.

In the situation where a noise source (possibly a vibrating structure) is radiating into an enclosure, the goal of an active control system is to minimize sound transmission into the coupled enclosure. In this case the global error criterion is potential energy; which is written as

$$E_p = \frac{1}{4\rho c^2}\int_V |p(\boldsymbol{r})|^2 \,\mathrm{d}\boldsymbol{r} \tag{2}$$

where ρ is the density and c the speed of sound within the acoustic fluid enclosed by the cavity, p the acoustic pressure and the integral is evaluated over the enclosure volume, V, and $\boldsymbol{r} = (x, y, z)$. The goal of this work is to construct a cost function for potential energy of the form in Eq. (1) which is independent of any structural parameters, i.e. the thickness, the boundary conditions, vibration amplitudes, etc. Ideally the result would then be a group of generalized orthogonal acoustic radiation functions, which are applicable to *any* noise source (structural or non-structural). As a direct consequence of the general nature of the generalized orthogonal radiation functions, the goal of the active control system is to measure and minimize these functions in all practical situations.

In this study it is assumed that there is 'weak coupling' between the generic noise source and the acoustic space. Therefore, if the source was a vibrating panel, the response of the panel can be described in terms of its *in vacuo* mode shape functions and the response of the acoustic space to be described in terms of the rigid-wall mode shape functions. This is a valid assumption where the structure encompasses a relatively large air filled space and has some degree of stiffness such that the radiation loading on the structure will be relatively small, and similarly the motion of the structure will not significantly alter the shape of the acoustic space [14].

With the assumption of weak coupling, the acoustic pressure at any location in the enclosed space can be expressed in terms of the rigid-wall acoustic mode shape functions of the cavity,

$$p(\boldsymbol{r}) = \sum_{i=1}^{\infty} p_i \phi_i(\boldsymbol{r}) \tag{3}$$

where p_i is the pressure amplitude of the ith acoustic mode and ϕ_i is the value of the associated mode shape function at the location $\boldsymbol{r}$ in space. Substituting Eq. (3) into Eq. (2), the acoustic potential energy is rewritten as

$$E_p = \frac{1}{4\rho c^2}\int_V \left(\sum p_i \phi_i(\boldsymbol{r})\right)^* \left(\sum p_j \phi_j(\boldsymbol{r})\right) \mathrm{d}\boldsymbol{r} \tag{4}$$

Using modal orthogonality of the acoustic modes within the cavity,

$$\int_V \phi_i(\boldsymbol{r})^* \phi_j(\boldsymbol{r}) \,\mathrm{d}\boldsymbol{r} = \begin{cases} 0, & i \neq j \\ \Lambda_i, & i = j \end{cases} \tag{5}$$

where Λ_i is the volume normalization of the ith acoustic mode. Using the orthogonality property and limiting consideration to N acoustic modes, the expression for the global error, acoustic potential energy is written as

$$E_p = \frac{1}{4\rho c^2}\sum_{i=1}^{N}\Lambda_i|p_i|^2 = \mathbf{p}^{\mathrm{H}}\mathbf{W}\mathbf{p} \tag{6}$$

where $\mathbf{p}$ is the vector of acoustic modal amplitudes and $\mathbf{W}$ is a diagonal weighting matrix, the terms in which are

$$W(i,i) = \frac{\Lambda_i}{4\rho c^2} \tag{7}$$

Equation (6) is in precisely the desired form as required in Eq. (1), however, the global error is merely in terms of the acoustic mode shapes of the cavity, $\mathbf{p}$; there is no description of how the radiation from some generic source is contributing to the acoustic modal amplitudes. Furthermore the expression in Eq. (6) is convenient should only acoustic sensors and actuators be used, however, such an approach can be inefficient as acoustic control sources typically have weak control authority over structural elements, and in the case where a structure is the source of the disturbance, direct structural control is more efficient [17]. What is then sought is some generalized relationship between the radiation of a non-structural source or a vibrating panel, and the acoustic modes of the cavity—which can be measured and controlled in the structural or acoustic domain. By replacing the structural source with an array of monopole sources, as conceptually illustrated in Fig. 1, the development of the orthogonal decomposition is constrained entirely to the acoustic domain. The starting point for the generalized approach is to expand the pressure radiated by a noise source (later a vibrating panel is considered in simulation) in terms of acoustic multipole radiation patterns, analogous to the decomposition of a structural velocity distribution in terms of *in vacuo* mode shape functions, sound pressure is then written as

$$p_{\mathrm{multi}}(\boldsymbol{r}) = \sum_{i=1}^{\infty} a_i\psi_i(\boldsymbol{r}) \tag{8}$$

where a_i is the amplitude of the ith multipole and $\psi_i(\boldsymbol{r})$ the radiation transfer function for the ith multipole between the origin and the location in space, $\boldsymbol{r}$. Previous work based the expansion of pressure radiation into a cavity in terms of vibration amplitudes or vibration patterns of the flexible panel, which are dependent on its boundary conditions, thickness, internal properties, etc. What is sought here is a generalized *acoustic-centric* approach to structure–cavity interaction, an approach which would be equally applicable to a non-structure source within a cavity. The real benefit in a generalized approach is that, instead of some structural source, an array of monopole sources (capable of mimicking *any* noise source) are used, accordingly the technique is applicable to any noise source. As conceptually illustrated in Fig. 1 the development of orthogonal patterns to the global error is based on fundamental acoustic sources—rather than structural sources which imply structural measurements. At the heart of the generalized development of radiation into a coupled enclosure is the derivation of radiation patterns based on in-phase/out-of-phase combinations of monopoles situated in an array over the noise source. To generate a given multipole pattern, the amplitudes of all the monopole sources in the array are fixed to be equal. Consider a single monopole in a baffle, the noise radiation defined by a point source is written as

$$q\frac{\mathrm{j}\omega\rho}{2\pi\boldsymbol{r}}\mathrm{e}^{-\mathrm{j}k\boldsymbol{r}} \tag{9}$$

where q is the volume velocity of the source, j the imaginary operator, ω frequency of radiated noise, k the wavenumber and $\boldsymbol{r}$ the distance from the location of the point source to the point of interest. While the assumption that the monopoles are in an infinite baffle is not strictly correct for this cavity situation, the approximation of monopole radiation is shown to be sufficient due to the positioning of the sensors, as will be discussed.

Consider now eight virtual monopole sources, which are used to mimic (replace) the acoustic radiation that is generated by some generic noise source radiating into the enclosure. The precise phasing of the monopoles in the array is defined by the Hadamard matrix which contains a set of orthogonal functions composed of ±1 [28,29]. A convenience of the Hadamard matrix is that it easily allows for the use of more monopoles in the decomposition development. To generate a given 'acoustic multipole radiation pattern' the amplitudes of the virtual sources are fixed to be equal. The phasing of the sources that form the acoustic multipoles, in the case of eight monopoles, is governed by the relationship

$$\begin{bmatrix} 1 & 1 & 1 & 1 & 1 & 1 & 1 & 1 \\ 1 & 1 & 1 & 1 & -1 & -1 & -1 & -1 \\ 1 & 1 & -1 & -1 & -1 & -1 & 1 & 1 \\ 1 & 1 & -1 & -1 & 1 & 1 & -1 & -1 \\ 1 & -1 & -1 & 1 & -1 & 1 & 1 & -1 \\ 1 & -1 & 1 & -1 & -1 & 1 & -1 & 1 \\ 1 & -1 & 1 & -1 & 1 & -1 & 1 & -1 \\ 1 & -1 & -1 & 1 & 1 & -1 & -1 & 1 \end{bmatrix} \begin{bmatrix} q_1 \\ q_2 \\ q_3 \\ q_4 \\ q_5 \\ q_6 \\ q_7 \\ q_8 \end{bmatrix} \tag{10}$$

Using the definition in Eq. (10) the set of radiation transfer functions to a point in space, which constitute the elements in a given row of $\psi_i(\boldsymbol{r})$ in Eq. (8) are written as follows:

$$\begin{bmatrix}\psi_1(\boldsymbol{r})\\ \psi_2(\boldsymbol{r})\\ \vdots\\ \psi_8(\boldsymbol{r})\end{bmatrix} = \begin{bmatrix}1&1&1&1&1&1&1&1\\ 1&1&1&1&-1&-1&-1&-1\\ 1&1&-1&-1&-1&-1&1&1\\ 1&1&-1&-1&1&1&-1&-1\\ 1&-1&-1&1&-1&1&1&-1\\ 1&-1&1&-1&-1&1&-1&1\\ 1&-1&1&-1&1&-1&1&-1\\ 1&-1&-1&1&1&-1&-1&1\end{bmatrix} \begin{bmatrix}\frac{\mathrm{j}\omega\rho}{2\pi r_1}\mathrm{e}^{-\mathrm{j}kr_1}\\ \frac{\mathrm{j}\omega\rho}{2\pi r_2}\mathrm{e}^{-\mathrm{j}kr_2}\\ \vdots\\ \frac{\mathrm{j}\omega\rho}{2\pi r_8}\mathrm{e}^{-\mathrm{j}kr_8}\end{bmatrix} \tag{11}$$

where r_1 is the distance from the first monopole to the measurement point of pressure.

In the multipole development it is inherently assumed that *all* sound radiation from the generic source is captured in the resulting set of acoustic multipoles. The precise accuracy of this assumption (and others used in the development) is the subject of the numerical simulation, however, as noted in Ref. [30] *any* set of orthogonal functions can be used in the decomposition of a, quadratic, global error criterion. Observe in Eq. (11) that the first row of the Hadamard matrix will result in the set of eight virtual monopoles being all in phase, creating a radiation pattern similar to that of a monopole. Other fundamental acoustic shapes are also observable on close inspection of the rows in the Hadamard matrix: dipoles (rows 2 and 7) and a quadrupole (row 6), etc.

In an enclosure, the coupling, that is the energy exchange, between the cavity and the source occurs at the boundary of the source. This presents some mathematical difficulties for the proposed multipole approach as over the surface of source (where the virtual sources at placed) the value of $\psi(\boldsymbol{r})$ becomes undefined. However, here the assumption will be made (and later tested in simulation) that an approximation of the coupling can be evaluated in the vicinity of the monopole sources, where the functions $\psi(\boldsymbol{r})$ become smooth.

The form of Eq. (11) provides no restriction for the placement of a set of acoustic sensors. However, to avoid simply measuring sound pressure which is dominated by the acoustic cavity modes (as the case would be if the sensors where placed at some distance from the panel) the sensors must be placed close to the vibrating panel. Withal, as will be clearly shown shortly, the acoustic measurements used to resolve the multipole amplitudes need to be taken close to where the acoustic and vibration fields interact, as this is where the energy exchange is taking place. In general (i.e. in cases where more or less sensors than virtual monopoles are used) the multipole amplitudes can be resolved using a matrix inversion or pseudo-inversion in a general sense as follows:

$$\boldsymbol{a} = \boldsymbol{\Psi}^{-1}\hat{\mathbf{p}} \tag{12}$$

where the vector $\hat{\mathbf{p}}$ contains a set of point sound pressure measurements. When the vector $\hat{\mathbf{p}}$ is measured very close to the panel and the microphones are situated at the locations of the virtual monopoles, then the measured pressures correspond to the virtual monopole amplitudes and thus the acoustic multipole amplitudes are simply equal to

$$\boldsymbol{a} = \{\mathbf{H}^{\mathrm{T}}\}^{-1}\hat{\mathbf{p}} \tag{13}$$

where $\mathbf{H}$ is the square Hadamard matrix. Should a set of structural sensors be placed at the virtual monopole locations the multipole amplitudes become

$$\boldsymbol{a} = \{\mathbf{H}^{\mathrm{T}}\}^{-1}\hat{\mathbf{v}} \tag{14}$$

where $\hat{\mathbf{v}}$ is the vector of structural measurements. Such an arrangement is similar to the structural sensing of the multipole approach for the acoustic free field, completed previously in experiments [23,31].

The resultant acoustic pressure at any location $p(\boldsymbol{r})$ in the enclosed space due to the radiation (which is decomposed into multipole radiation patterns) into the cavity from a generic source is defined by the Green's function response equation,

$$p(\boldsymbol{r}) = \mathrm{j}\rho\omega \int_S G_a(\vec{\boldsymbol{x}}|\boldsymbol{r})\hat{p}_{\mathrm{multi}}(\vec{\boldsymbol{x}})\,\mathrm{d}\vec{\boldsymbol{x}} \tag{15}$$

where $\hat{p}_{\mathrm{multi}}(\vec{\boldsymbol{x}})$ is the acoustic source strength in units of volume velocity per unit volume calculated from Eq. (8) at the location $\vec{\boldsymbol{x}}$ on the enclosing structure, defined in Eq. (8). Green's function for the cavity is written as

$$G_a(\vec{\boldsymbol{x}}|\boldsymbol{r}) = \sum_{i=1}^{\infty} \frac{\phi_i(\vec{\boldsymbol{x}})\phi_i(\boldsymbol{r})}{\Lambda_i(\kappa_i^2 - k^2)} \tag{16}$$

where κ_i is the complex (damped) eigenvalue of the ith acoustic modes. Should a planar radiator be considered as the noise source the integration in Eq. (15) is over the surface S of the radiator to reflect the true nature of the coupling between sound emanating from the panel and the enclosure modes. Consider a generic planar radiator, as this is a common practical

problem; the complex amplitude of the ith acoustic mode can be expressed as

$$p_i = \mathrm{j}\rho\omega \int_S \frac{\phi_i(\vec{\boldsymbol{x}})}{\Lambda_i(\kappa_i^2 - k^2)} \hat{p}_{\mathrm{multi}}(\vec{\boldsymbol{x}})\, \mathrm{d}\vec{\boldsymbol{x}} \tag{17}$$

Using the expanded terms of the acoustic multipole functions, a in Eq. (8), the amplitude of the ith acoustic mode can be reexpressed as

$$\begin{aligned} p_i &= \frac{\mathrm{j}\rho\omega}{\Lambda_i(\kappa_i^2 - k^2)} \int_S \sum_{j=1}^{N_s} \phi_i(\vec{\boldsymbol{x}})\psi_j(\vec{\boldsymbol{x}}) a_j\, \mathrm{d}\vec{\boldsymbol{x}} \\ &= \frac{\mathrm{j}\rho\omega}{\Lambda_i(\kappa_i^2 - k^2)} \sum_{j=1}^{N_s} \boldsymbol{\beta}_{i,j} a_j \end{aligned} \tag{18}$$

where $\boldsymbol{\beta}_{i,j}$ is the non-dimensional modal coupling coefficient for the ith acoustic mode and the jth multipole radiation pattern,

$$\boldsymbol{\beta}_{i,j} = \int_S \phi_i(\vec{\boldsymbol{x}})\psi_j(\vec{\boldsymbol{x}})\, \mathrm{d}\vec{\boldsymbol{x}} \tag{19}$$

and there are N_s multipoles used to mimic the total radiation by the rectangular panel. Should the practical situation under consideration not be a planar radiator this approach is still applicable, simply the integral in Eq. (19) will be over a different space. The acoustic modal amplitudes of the cavity defined in Eq. (18) can thus be rewritten as a matrix expression, where the complex amplitude of the ith acoustic mode is equal to

$$p_i = \mathbf{z}_{a,i}^{\mathrm{T}} \boldsymbol{a} \tag{20}$$

where $\boldsymbol{a}$ is the $(N_s \times 1)$ vector of acoustic multipole amplitudes and $z_{a,i}$ is the $(N_s \times 1)$ vector of radiation transfer function between the acoustic multipoles and the ith acoustic mode, the terms of which are defined by

$$z_{a,i} = \frac{\mathrm{j}\rho\omega}{\Lambda_i(\kappa_i^2 - k^2)} \boldsymbol{\beta}_{i,j} \tag{21}$$

Combining Eqs. (15)–(21) the vector of N_a acoustic modal amplitudes $\mathbf{p}$ is defined by the expression

$$\mathbf{p} = \mathbf{Z}_a \boldsymbol{a} \tag{22}$$

where $\mathbf{Z}_a$ is the $(N_a \times N_s)$ matrix of radiation transfer vectors,

$$\mathbf{Z}_a = \begin{bmatrix} z_{a,1}^{\mathrm{T}} \\ z_{a,2}^{\mathrm{T}} \\ \vdots \\ z_{a,N_s}^{\mathrm{T}} \end{bmatrix} \tag{23}$$

Equation (22) can be substituted into Eq. (6) to express the acoustic potential energy in the form of Eq. (1), where the transfer matrix $\mathbf{A}$ is defined by the relationship

$$\mathbf{A} = \mathbf{Z}_a^{*} \mathbf{W} \mathbf{Z}_a^{\mathrm{T}} \tag{24}$$

such that the (m,n)th term is equal to

$$\mathbf{A}(m,n) = \sum_{i=1}^{N_a} \frac{\mathrm{j}\rho k^2 S^2}{4\Lambda_i |\kappa_i^2 - k^2|^2} \boldsymbol{\beta}_{i,m} \boldsymbol{\beta}_{i,n} \tag{25}$$

Observe that the terms in the transfer matrix are strongly frequency dependent, governed by the frequency of excitation and the admittance $(\kappa_i^2 - k^2)^{-1}$. The eigenvalues of the transfer matrix will therefore peak at resonances of the acoustic modes to which the acoustic multipoles couple. The peak in eigenvalues at each cavity mode will be related to the acoustic multipole pattern that has the greatest coupling coefficient to the cavity mode. Equation (25) shows that the error weighting matrix, $\mathbf{A}$, is not constrained to be diagonal. However, it is square and symmetric, hence it can be diagonalized using an orthonormal transformation:

$$\mathbf{A} = \mathbf{Q} \boldsymbol{\Lambda} \mathbf{Q}^{-1} \tag{26}$$

where the columns of $\mathbf{Q}$ are the eigenvectors of $\mathbf{A}$ and $\boldsymbol{\Lambda}$ is a diagonal matrix of the associated eigenvalues. Combining all of this into the same form as Eq. (1), the global error, acoustic potential energy within the cavity, can be written as

$$E_p \approx \hat{\mathbf{p}}^{\mathrm{H}} \{\boldsymbol{\Psi}^{-1}\}^{\mathrm{H}} \mathbf{Q} \boldsymbol{\Lambda} \mathbf{Q}^{-1} \boldsymbol{\Psi}^{-1} \hat{\mathbf{p}} \tag{27}$$

With this decoupling the modal filtering weights used to measure the generalized orthogonal contributors to acoustic potential energy are defined by $\mathbf{Q}^{-1}\mathbf{\Psi}^{-1}$, and the amplitudes of the orthogonal contributors (the orthogonal acoustic multipole amplitudes) to be used as error signals in a control implementation are then written as

$$\boldsymbol{a}_{\text{ortho}} = \mathbf{Q}^{-1}\mathbf{\Psi}^{-1}\hat{\mathbf{p}} \tag{28}$$

When sensors are positioned at the location of the virtual monopoles, the virtual monopole amplitudes are measured directly (using structural or acoustic measurements), Eq. (28), the estimate of the orthogonal acoustic multipole amplitudes becomes

$$\boldsymbol{a}_{\text{ortho}} = \mathbf{Q}^{-1}\{\mathbf{H}^{\text{T}}\}^{-1}\hat{\mathbf{p}} \tag{29}$$

In the case of vibration sensors positioned at the virtual monopole locations, the estimate of the orthogonal acoustic multipole amplitudes becomes

$$\boldsymbol{a}_{\text{ortho}} = \mathbf{Q}^{-1}\{\mathbf{H}^{\text{T}}\}^{-1}\hat{\mathbf{v}} \tag{30}$$

Equations (28)–(30) represent a target for a sensing system and the ideal situation for an active controller where the measured errors, $\boldsymbol{a}_{\text{ortho}}$, contribute orthogonally to the global cost function. Implementation of the modal filtering scheme to measure the orthogonal contributors to acoustic potential energy is then straightforward: measure the pressure at the sensing locations, multiply the vector of pressure measurements by the fixed terms in $\mathbf{Q}^{-1}\mathbf{\Psi}^{-1}$ (yielding a greatly reduced number of outputs), and pass the handful of resulting signals through a set of filters with characteristics defined by $\mathbf{\Lambda}$ prior to input to the controller.

3. Simulation

3.1. Frequency characteristics

To investigate the problem of measuring and minimizing the generalized contributors (acoustic multipoles) to achieve a reduction in the global error we now specialize the problem. Consider an enclosure of dimensions $0.39 \times 0.68 \times 0.9\,\text{m}$ ($l_x \times l_y \times l_z$), as illustrated in Fig. 2. At one end of the enclosure is a flexible panel with a thickness of 0.004 m. For the purpose of the simulation, simply supported boundary conditions are used (i.e. such that the panel resonance frequencies can be calculated). The frequency range of interest for this work is up to 700 Hz.

A structural source is chosen for several reasons. Firstly there is a significant amount of accepted literature describing the acoustic radiation of such a source. Secondly the maximum possible attenuation of the global error can be easily calculated for such a noise source based on the input disturbance and the location and type of control actuator(s). Should a non-structural source be chosen the precise sound pressure radiation characteristics of the source would firstly need to be illustrated, and then a method for determining the maximum possible attenuation proposed; both of which would present more unanswered questions than simulations based on the well-understood vibrating panel. More importantly though, the choice of a structural source will not compromise the generalized aspects of the sensing system design and thus the simulation results because the generalized modal filter weights were developed *independent* of the structural source and depend on the decomposition of the noise source by an array of monopole sources, a result that has been proved experimentally [25–27]. The sensing system just decomposes any radiation presented at the sensors into set of orthogonal contributors to acoustic potential energy, a set of orthogonal contributors that are for *any* noise source; structural or non-structural sources alike. The heart of the issue is the decomposition of sound radiation into a set of radiation patterns based on an array of monopoles i.e. Eq. (8).

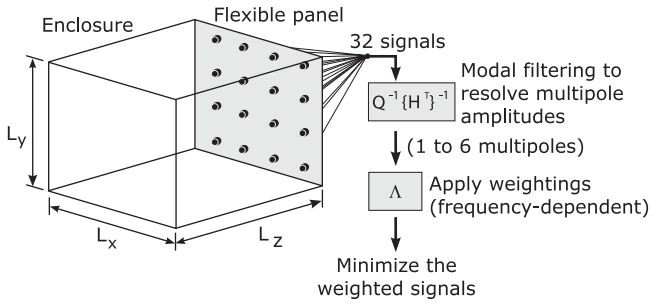

Fig. 2. System geometry and sensor arrangement for simulation.

Table 1
Enclosure resonances below 700 Hz.

Mode (L, M, N)	Resonance frequency (Hz)
0, 0, 0	0
0, 0, 1	190.6
0, 1, 0	252.2
0, 1, 1	316.1
0, 0, 2	381.1
1, 0, 0	439.7
0, 1, 2	457.0
1, 0, 1	479.3
0, 2, 0	504.4
1, 1, 0	506.9
0, 2, 1	539.2
1, 1, 1	541.6
0, 0, 3	571.7
1, 0, 2	581.9
0, 1, 3	624.8
0, 2, 2	632.2
1, 1, 2	634.2
1, 2, 0	669.2
1, 2, 1	695.8

Table 2
Panel resonances below 700 Hz.

Mode (M_x, N_y)	Resonance frequency (Hz)
1,1	85.6
1,2	149.1
1,3	255.0
2,1	278.8
2,2	342.3
1,4	403.3
2,3	448.2
1,5	593.9
2,4	596.5
3,1	600.8
3,2	664.3

The mode shape function of the rectangular cavity with rigid walls is

$$\phi_{L,M,N}(x,y,z) = \cos\frac{L\pi x}{L_x}\cos\frac{M\pi y}{L_y}\cos\frac{N\pi z}{L_z} \tag{31}$$

with the associated resonance frequencies defined by the relationship

$$\omega_{L,M,N} = c\pi\sqrt{\left(\frac{L}{L_x}\right)^2 + \left(\frac{M}{L_y}\right)^2 + \left(\frac{N}{L_z}\right)^2} \tag{32}$$

Table 1 contains the cavity modes and Table 2 the panel modes below 700 Hz.

As mentioned the nature of the **A** matrix plays an important role in determining the precise characteristics of the active control setup, i.e. the number of errors that need to be measured and controlled. Recall that the eigenvalues (contained in $\mathbf{\Lambda}$, Eq. (26)) of **A** are directly proportional to the radiation efficiency of the radiation patterns, thus the eigenvalues indicate how many orthogonal patterns contribute to the global error; and subsequently the number of errors that should be measured and controlled. Recall that the corresponding eigenvectors define the orthogonal acoustic radiation patterns into the cavity, which in this case must be measured over the surface of the radiated panel. In the previous section it was noted that both of these quantities have some level of frequency dependency, the nature of this dependence and its influence on the global attenuation when ignored is examined.

Consider now 32 monopoles distributed evenly over the surface of the panel in a four by eight array. The separation of the monopoles is 0.078 m in the x-axis and 0.0755 m in the y-axis. In this case 32 virtual monopoles have been considered because beyond this number it was observed that the most important eigenvalues over the considered frequency range changed very little when more monopoles are included. The Hadamard matrix for this case is

$$\mathbf{H} = \begin{bmatrix}
1 & 1 & 1 & 1 & 1 & 1 & 1 & 1 & 1 & 1 & 1 & 1 & 1 & 1 & 1 & 1 & 1 & 1 & 1 & 1 & 1 & 1 & 1 & 1 & 1 & 1 & 1 & 1 & 1 & 1 & 1 & 1 \\
1 & -1 & 1 & -1 & 1 & -1 & 1 & -1 & 1 & -1 & 1 & -1 & 1 & -1 & 1 & -1 & 1 & -1 & 1 & -1 & 1 & -1 & 1 & -1 & 1 & -1 & 1 & -1 & 1 & -1 & 1 & -1 \\
1 & 1 & -1 & -1 & 1 & 1 & -1 & -1 & 1 & 1 & -1 & -1 & 1 & 1 & -1 & -1 & 1 & 1 & -1 & -1 & 1 & 1 & -1 & -1 & 1 & 1 & -1 & -1 & 1 & 1 & -1 & -1 \\
1 & -1 & -1 & 1 & 1 & -1 & -1 & 1 & 1 & -1 & -1 & 1 & 1 & -1 & -1 & 1 & 1 & -1 & -1 & 1 & 1 & -1 & -1 & 1 & 1 & -1 & -1 & 1 & 1 & -1 & -1 & 1 \\
1 & 1 & 1 & 1 & -1 & -1 & -1 & -1 & 1 & 1 & 1 & 1 & -1 & -1 & -1 & -1 & 1 & 1 & 1 & 1 & -1 & -1 & -1 & -1 & 1 & 1 & 1 & 1 & -1 & -1 & -1 & -1 \\
1 & -1 & 1 & -1 & -1 & 1 & -1 & 1 & 1 & -1 & 1 & -1 & -1 & 1 & -1 & 1 & 1 & -1 & 1 & -1 & -1 & 1 & -1 & 1 & 1 & -1 & 1 & -1 & -1 & 1 & -1 & 1 \\
1 & 1 & -1 & -1 & -1 & -1 & 1 & 1 & 1 & 1 & -1 & -1 & -1 & -1 & 1 & 1 & 1 & 1 & -1 & -1 & -1 & -1 & 1 & 1 & 1 & 1 & -1 & -1 & -1 & -1 & 1 & 1 \\
1 & -1 & -1 & 1 & -1 & 1 & 1 & -1 & 1 & -1 & -1 & 1 & -1 & 1 & 1 & -1 & 1 & -1 & -1 & 1 & -1 & 1 & 1 & -1 & 1 & -1 & -1 & 1 & -1 & 1 & 1 & -1 \\
1 & 1 & 1 & 1 & 1 & 1 & 1 & 1 & -1 & -1 & -1 & -1 & -1 & -1 & -1 & -1 & 1 & 1 & 1 & 1 & 1 & 1 & 1 & 1 & -1 & -1 & -1 & -1 & -1 & -1 & -1 & -1 \\
1 & -1 & 1 & -1 & 1 & -1 & 1 & -1 & -1 & 1 & -1 & 1 & -1 & 1 & -1 & 1 & 1 & -1 & 1 & -1 & 1 & -1 & 1 & -1 & -1 & 1 & -1 & 1 & -1 & 1 & -1 & 1 \\
1 & 1 & -1 & -1 & 1 & 1 & -1 & -1 & -1 & -1 & 1 & 1 & -1 & -1 & 1 & 1 & 1 & 1 & -1 & -1 & 1 & 1 & -1 & -1 & -1 & -1 & 1 & 1 & -1 & -1 & 1 & 1 \\
1 & -1 & -1 & 1 & 1 & -1 & -1 & 1 & -1 & 1 & 1 & -1 & -1 & 1 & 1 & -1 & 1 & -1 & -1 & 1 & 1 & -1 & -1 & 1 & -1 & 1 & 1 & -1 & -1 & 1 & 1 & -1 \\
1 & 1 & 1 & 1 & -1 & -1 & -1 & -1 & -1 & -1 & -1 & -1 & 1 & 1 & 1 & 1 & 1 & 1 & 1 & 1 & -1 & -1 & -1 & -1 & -1 & -1 & -1 & -1 & 1 & 1 & 1 & 1 \\
1 & -1 & 1 & -1 & -1 & 1 & -1 & 1 & -1 & 1 & -1 & 1 & 1 & -1 & 1 & -1 & 1 & -1 & 1 & -1 & -1 & 1 & -1 & 1 & -1 & 1 & -1 & 1 & 1 & -1 & 1 & -1 \\
1 & 1 & -1 & -1 & -1 & -1 & 1 & 1 & -1 & -1 & 1 & 1 & 1 & 1 & -1 & -1 & 1 & 1 & -1 & -1 & -1 & -1 & 1 & 1 & -1 & -1 & 1 & 1 & 1 & 1 & -1 & -1 \\
1 & -1 & -1 & 1 & -1 & 1 & 1 & -1 & -1 & 1 & 1 & -1 & 1 & -1 & -1 & 1 & 1 & -1 & 1 & 1 & -1 & -1 & 1 & 1 & -1 & -1 & 1 & 1 & -1 & -1 & 1 & 1 \\
1 & 1 & 1 & 1 & 1 & 1 & 1 & 1 & 1 & 1 & 1 & 1 & 1 & 1 & 1 & 1 & -1 & -1 & -1 & -1 & -1 & -1 & -1 & -1 & -1 & -1 & -1 & -1 & -1 & -1 & -1 & -1 \\
1 & -1 & 1 & -1 & 1 & -1 & 1 & -1 & 1 & -1 & 1 & -1 & 1 & -1 & 1 & -1 & -1 & 1 & -1 & 1 & -1 & 1 & -1 & 1 & -1 & 1 & -1 & 1 & -1 & 1 & -1 & 1 \\
1 & 1 & -1 & -1 & 1 & 1 & -1 & -1 & 1 & 1 & -1 & -1 & 1 & 1 & -1 & -1 & -1 & -1 & 1 & 1 & -1 & -1 & 1 & 1 & -1 & -1 & 1 & 1 & -1 & -1 & 1 & 1 \\
1 & -1 & -1 & 1 & 1 & -1 & -1 & 1 & 1 & -1 & -1 & 1 & 1 & -1 & -1 & 1 & -1 & 1 & 1 & -1 & -1 & 1 & 1 & -1 & -1 & 1 & 1 & -1 & -1 & 1 & 1 & -1 \\
1 & 1 & 1 & 1 & -1 & -1 & -1 & -1 & 1 & 1 & 1 & 1 & -1 & -1 & -1 & -1 & -1 & -1 & -1 & -1 & 1 & 1 & 1 & 1 & -1 & -1 & -1 & -1 & 1 & 1 & 1 & 1 \\
1 & -1 & 1 & -1 & -1 & 1 & -1 & 1 & 1 & -1 & 1 & -1 & -1 & 1 & -1 & 1 & -1 & 1 & -1 & 1 & 1 & -1 & 1 & -1 & -1 & 1 & -1 & 1 & 1 & -1 & 1 & -1 \\
1 & 1 & -1 & -1 & -1 & -1 & 1 & 1 & 1 & 1 & -1 & -1 & -1 & -1 & 1 & 1 & -1 & -1 & 1 & 1 & 1 & 1 & -1 & -1 & -1 & -1 & 1 & 1 & 1 & 1 & -1 & -1 \\
1 & -1 & -1 & 1 & -1 & 1 & 1 & -1 & 1 & -1 & -1 & 1 & -1 & 1 & 1 & -1 & -1 & 1 & 1 & -1 & 1 & -1 & -1 & 1 & -1 & 1 & 1 & -1 & 1 & -1 & -1 & 1 \\
1 & 1 & 1 & 1 & 1 & 1 & 1 & 1 & -1 & -1 & -1 & -1 & -1 & -1 & -1 & -1 & -1 & -1 & -1 & -1 & -1 & -1 & -1 & -1 & 1 & 1 & 1 & 1 & 1 & 1 & 1 & 1 \\
1 & -1 & 1 & -1 & 1 & -1 & 1 & -1 & -1 & 1 & -1 & 1 & -1 & 1 & -1 & 1 & -1 & 1 & -1 & 1 & -1 & 1 & -1 & 1 & 1 & -1 & 1 & -1 & 1 & -1 & 1 & -1 \\
1 & 1 & -1 & -1 & 1 & 1 & -1 & -1 & -1 & -1 & 1 & 1 & -1 & -1 & 1 & 1 & -1 & -1 & 1 & 1 & -1 & -1 & 1 & 1 & 1 & 1 & -1 & -1 & 1 & 1 & -1 & -1 \\
1 & -1 & -1 & 1 & 1 & -1 & -1 & 1 & -1 & 1 & 1 & -1 & -1 & 1 & 1 & -1 & -1 & 1 & 1 & -1 & -1 & 1 & 1 & -1 & 1 & -1 & -1 & 1 & 1 & -1 & -1 & 1 \\
1 & 1 & 1 & 1 & -1 & -1 & -1 & -1 & -1 & -1 & -1 & -1 & 1 & 1 & 1 & 1 & -1 & -1 & -1 & -1 & 1 & 1 & 1 & 1 & 1 & 1 & 1 & 1 & -1 & -1 & -1 & -1 \\
1 & -1 & 1 & -1 & -1 & 1 & -1 & 1 & -1 & 1 & -1 & 1 & 1 & -1 & 1 & -1 & -1 & 1 & -1 & 1 & 1 & -1 & 1 & -1 & 1 & -1 & 1 & -1 & -1 & 1 & -1 & 1 \\
1 & 1 & -1 & -1 & -1 & -1 & 1 & 1 & -1 & -1 & 1 & 1 & 1 & 1 & -1 & -1 & -1 & -1 & 1 & 1 & 1 & 1 & -1 & -1 & 1 & 1 & -1 & -1 & -1 & -1 & 1 & 1 \\
1 & -1 & -1 & 1 & -1 & 1 & 1 & -1 & -1 & 1 & 1 & -1 & 1 & -1 & -1 & 1 & -1 & 1 & 1 & -1 & 1 & -1 & -1 & 1 & -1 & 1 & 1 & -1 & 1 & -1 & -1 & 1
\end{bmatrix} \tag{33}$$

The evaluation of **A** requires the evaluation of the coupling matrix, $\boldsymbol{\beta}_{i,j}$ on the surface of the vibrating panel, where the acoustic modes of the enclosure actually impinge on the radiating surface. However, $\psi(\boldsymbol{r})$, Eq. (11), is undefined over the surface of the panel at the virtual monopole locations. The situation here shows some characteristics of the 'minimum sphere' modelling phenomena where an acoustic field is represented by a number of virtual sources. In such modelling situations there exists an area, or volume, where the error is small (outside the 'minimum sphere') but inside the acoustic field is not necessarily accurately represented [32,33]. In the application here the minimum sphere issue is connected to the value for kr chosen to evaluate $\psi(\boldsymbol{r})$. By choosing a distance close to the panel surface (0.1 m) to satisfy the idea that $\psi(\boldsymbol{r})$ should be evaluated over the surface of the noise source and a frequency of 1 Hz, the influence of the minimum sphere phenomena will be minimized, as the minimum sphere, r_m for a given wavenumber, k will be approximately equal to [33]

$$r_m \geq \frac{2\pi}{\frac{343}{k}} \tag{34}$$

Furthermore, empirically speaking at a frequency of 1 Hz ($k = 0.018$) and a distance of 0.1 m from the noise source the function $\psi(\boldsymbol{r})$ is smooth (there are no large variations in the function over small spatial variations). A low kr, $\psi(\boldsymbol{r})$ is observed to represent simple radiation patterns similar to monopoles, dipoles, etc., at higher kr the number of peaks and troughs, over the same surface in space, is significantly more. The $\psi(\boldsymbol{r})$ is frequency dependent, however, ultimately it is assumed that the acoustic patterns calculated under these conditions, and the resulting values of $\boldsymbol{\beta}_{i,j}$ are assumed constant for the entire frequency range. Should these assumptions be unreasonable the achievable attenuation, when minimizing the orthogonal multipoles, will be less than the maximum possible for the given actuator arrangement. These issues are examined in the following sections of the article. The matrix $\boldsymbol{\beta}_{i,j}$ at 1 Hz for the given monopole arrangement is

$$\boldsymbol{\beta}(m,n)_{1\text{ Hz}} = \begin{bmatrix}
0.2125 & -0.2125 & 0 & 0 & 0.2125 & 0 & 0 & 0 & -0.017 & 0 & 0.017 & 0 & -0.2125 & 0 & 0 & -0.017 & 0 & 0 & 0 \\
0 & 0 & 0 & 0 & 0 & 0.1116 & 0 & -0.1116 & 0 & 0 & 0 & 0 & 0 & 0.1116 & 0 & 0 & 0 & -0.0149 & 0.0149 \\
0 & 0 & 0 & 0 & 0 & 0.1236 & 0 & -0.1236 & 0 & 0 & 0 & 0 & 0 & 0.1236 & 0 & 0 & 0 & -0.0168 & 0.0168 \\
-0.0695 & 0.0695 & 0 & 0 & -0.0695 & 0 & 0 & 0 & 0.0091 & 0 & -0.0091 & 0 & 0.0695 & 0 & 0 & 0.0091 & 0 & 0 & 0 \\
0 & 0 & 0.0966 & -0.0966 & 0 & 0 & 0.0966 & 0 & 0 & 0 & 0 & 0 & 0 & 0 & -0.0966 & 0 & 0 & 0 & 0 \\
0 & 0 & 0 & 0 & 0 & 0 & 0 & 0 & 0 & 0.0477 & 0 & -0.0477 & 0 & 0 & 0 & 0 & 0.0477 & 0 & 0 \\
0 & 0 & 0 & 0 & 0 & 0 & 0 & 0 & 0 & 0.0536 & 0 & -0.0536 & 0 & 0 & 0 & 0 & 0.0536 & 0 & 0 \\
0 & 0 & -0.0219 & 0.0219 & 0 & 0 & -0.0219 & 0 & 0 & 0 & 0 & 0 & 0 & 0 & 0.0219 & 0 & 0 & 0 & 0 \\
0 & 0 & 0.0955 & -0.0955 & 0 & 0 & 0.0955 & 0 & 0 & 0 & 0 & 0 & 0 & 0 & -0.0955 & 0 & 0 & 0 & 0 \\
0 & 0 & 0 & 0 & 0 & 0 & 0 & 0 & 0 & 0.048 & 0 & -0.048 & 0 & 0 & 0 & 0 & 0.048 & 0 & 0 \\
0 & 0 & 0 & 0 & 0 & 0 & 0 & 0 & 0 & 0.0532 & 0 & -0.0532 & 0 & 0 & 0 & 0 & 0.0532 & 0 & 0 \\
0 & 0 & -0.0216 & 0.0216 & 0 & 0 & -0.0216 & 0 & 0 & 0 & 0 & 0 & 0 & 0 & 0.0216 & 0 & 0 & 0 & 0 \\
-0.0518 & 0.0518 & 0 & 0 & -0.0518 & 0 & 0 & 0 & 0.0101 & 0 & -0.0101 & 0 & 0.0518 & 0 & 0 & 0.0101 & 0 & 0 & 0 \\
0 & 0 & 0 & 0 & 0 & -0.0166 & 0 & 0.0166 & 0 & 0 & 0 & 0 & 0 & -0.0166 & 0 & 0 & 0 & 0.0026 & -0.0026 \\
0 & 0 & 0 & 0 & 0 & -0.0186 & 0 & 0.0186 & 0 & 0 & 0 & 0 & 0 & -0.0186 & 0 & 0 & 0 & 0.0027 & -0.0027 \\
0.0073 & -0.0073 & 0 & 0 & 0.0073 & 0 & 0 & 0 & -0.0011 & 0 & 0.0011 & 0 & -0.0073 & 0 & 0 & -0.0011 & 0 & 0 & 0 \\
0 & 0 & 0.1224 & -0.1224 & 0 & 0 & 0.1224 & 0 & 0 & 0 & 0 & 0 & 0 & 0 & -0.1224 & 0 & 0 & 0 & 0 \\
0 & 0 & 0 & 0 & 0 & 0 & 0 & 0 & 0 & 0.069 & 0 & -0.069 & 0 & 0 & 0 & 0 & 0.069 & 0 & 0 \\
0 & 0 & 0 & 0 & 0 & 0 & 0 & 0 & 0 & 0.0764 & 0 & -0.0764 & 0 & 0 & 0 & 0 & 0.0764 & 0 & 0 \\
0 & 0 & -0.0336 & 0.0336 & 0 & 0 & -0.0336 & 0 & 0 & 0 & 0 & 0 & 0 & 0 & 0.0336 & 0 & 0 & 0 & 0 \\
-0.05 & 0.05 & 0 & 0 & -0.05 & 0 & 0 & 0 & 0.0693 & 0 & -0.0693 & 0 & 0.05 & 0 & 0 & 0.0693 & 0 & 0 & 0 \\
0 & 0 & 0 & 0 & 0 & -0.0175 & 0 & 0.0175 & 0 & 0 & 0 & 0 & 0 & -0.0175 & 0 & 0 & 0 & 0.0412 & -0.0412 \\
0 & 0 & 0 & 0 & 0 & -0.0189 & 0 & 0.0189 & 0 & 0 & 0 & 0 & 0 & -0.0189 & 0 & 0 & 0 & 0.0464 & -0.0464 \\
0.009 & -0.009 & 0 & 0 & 0.009 & 0 & 0 & 0 & -0.0164 & 0 & 0.0164 & 0 & -0.009 & 0 & 0 & -0.0164 & 0 & 0 & 0 \\
-0.0462 & 0.0462 & 0 & 0 & -0.0462 & 0 & 0 & 0 & 0.0783 & 0 & -0.0783 & 0 & 0.0462 & 0 & 0 & 0.0783 & 0 & 0 & 0 \\
0 & 0 & 0 & 0 & 0 & -0.0163 & 0 & 0.0163 & 0 & 0 & 0 & 0 & 0 & -0.0163 & 0 & 0 & 0 & 0.0507 & -0.0507 \\
0 & 0 & 0 & 0 & 0 & -0.0173 & 0 & 0.0173 & 0 & 0 & 0 & 0 & 0 & -0.0173 & 0 & 0 & 0 & 0.0565 & -0.0565 \\
0.009 & -0.009 & 0 & 0 & 0.009 & 0 & 0 & 0 & -0.0208 & 0 & 0.0208 & 0 & -0.009 & 0 & 0 & -0.0208 & 0 & 0 & 0 \\
0 & 0 & -0.0528 & 0.0528 & 0 & 0 & -0.0528 & 0 & 0 & 0 & 0 & 0 & 0 & 0 & 0.0528 & 0 & 0 & 0 & 0 \\
0 & 0 & 0 & 0 & 0 & 0 & 0 & 0 & 0 & -0.0236 & 0 & 0.0236 & 0 & 0 & 0 & 0 & -0.0236 & 0 & 0 \\
0 & 0 & 0 & 0 & 0 & 0 & 0 & 0 & 0 & -0.0263 & 0 & 0.0263 & 0 & 0 & 0 & 0 & -0.0263 & 0 & 0 \\
0 & 0 & 0.0101 & -0.0101 & 0 & 0 & 0.0101 & 0 & 0 & 0 & 0 & 0 & 0 & 0 & -0.0101 & 0 & 0 & 0 & 0
\end{bmatrix} \tag{35}$$

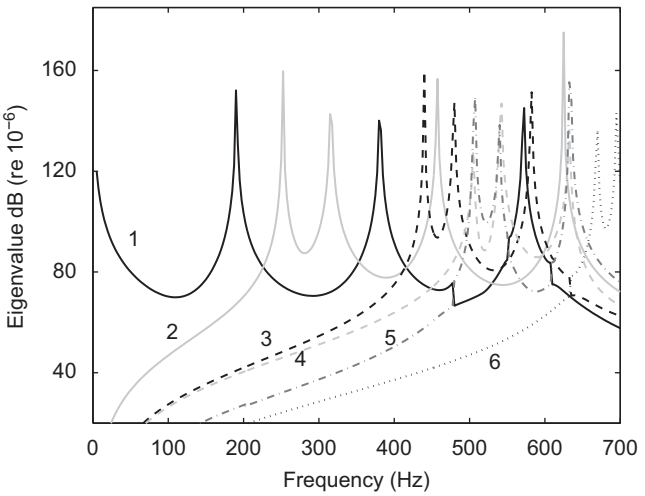

Fig. 3. Eigenvalues of the **A** as a function of frequency.

Observe in Eq. (35) that for each of the columns (the cavity modes) there is one multipole which often couples to the cavity mode significantly more than any other. Based on Eq. (25) then it is expected that the most important radiation pattern at each cavity mode will strongly resemble the corresponding multipole with the best coupling. Illustrated in Fig. 3 are the eigenvalues of **A** (Eq. (25)) over the frequency range 5–700 Hz. It is important to note that these eigenvalue amplitudes are sorted based on the eigenvector, accordingly the most efficient radiation pattern (recall the patterns are determined by the eigenvectors) at 10 Hz is the second most efficient shape at 300 Hz. From this point on when an orthogonal radiation pattern is referred to as the first, second, etc., these numerical descriptions are based on the order of radiation efficiency calculated at 5 Hz.

There is some variation of the eigenvectors of **A** over the frequency range 5–700 Hz, however, it is small enough to neglect. Such an assumption can be tested by comparing the achievable attenuation in comparison to the maximum theoretical possible for a given control arrangement; as will be done in the next section.

One curious characteristic of Fig. 3 is that the eigenvalue variation is not entirely smooth, observe the sharp swapping of eigenvector order. Observe that, the first and the fifth orthogonal radiation patterns swap at 480 Hz. Later, at 550 Hz they swap back again. The first and fifth radiation patterns later swap again, at 610 Hz. The third and sixth radiation patterns also swap, at 634 Hz. On two occasions the swapping occurs at a cavity mode frequency (though at amplitudes far below the eigenvalue at the peak). Exactly why this sharp swapping occurs is difficult to explain as the plotted data are a result of the inner workings of singular value decomposition on a matrix, **A**, that varies with frequency. It is important to observe that in each case the swap occurs near a trough of the eigenvalue; away from the peaks where maximum contribution to the global error occurs. Based on the values of $\boldsymbol{\beta}_{i,j}$ in Eq. (35) it is clear that the swap present in the figure matches the physical system. This point is observable in $\boldsymbol{\beta}_{i,j}$ as the multipole radiation patterns (the rows in $\boldsymbol{\beta}_{i,j}$) that couple the best to cavity modes (the columns in $\boldsymbol{\beta}_{i,j}$) 1, 2 and 5 are not the same as the ones that couple the best to cavity modes 9 and 10 (columns 9 and 10 of $\boldsymbol{\beta}_{i,j}$). Therefore the eigenvectors associated with the highest eigenvalue near the 1st, 2nd and 5th cavity resonance frequencies must be dominated by different acoustic multipoles than the eigenvector associated with the highest eigenvalue at the 9th and 10th cavity mode.

Observe that over the plotted frequency range there are only six orthogonal radiation patterns that will contribute to the global error within the cavity. Illustrated in Fig. 4 are these six orthogonal radiation patterns, evaluated at 1 Hz. Observe that the most efficient orthogonal pattern is monopole like (and is dominated by the contribution of the multipole corresponding to the first row of the Hadamard matrix), the second and third patterns are dipole like and the fourth quadrupole like. For the remainder, as the order increases, so does the complexity of the orthogonal shape. Even though the theoretical development of generalized orthogonal contributors here is for an acoustic enclosure, the orthogonal radiation patterns illustrated in Fig. 4 are remarkably similar to those also based on the multipole technique, applied in the acoustic free field [26]. The X and O that is marked on each of the radiation patterns in Fig. 4 shows the location of the disturbance and control source locations used in the next section. It is important to mention that the orthogonal radiation patterns themselves are independent of any excitation positions.

Returning to Fig. 3, observe the coupling between the orthogonal radiation patterns and the cavity modes is very selective, which is a consequence of the contents in $\boldsymbol{\beta}_{i,j}$ (Eq. (35)). The orthogonal shapes in Fig. 4 illustrate why the coupling is so selective, as the shapes can be classified in a similar way to vibration modes in terms of their modal indices, which indicate the number of peaks in the mode shape-along each axis. Observe that the first acoustic radiation pattern couples well with the cavity modes $0,0,N$ (L,M,N), where $N=1,2,\ldots$; the second acoustic radiation pattern couples well with the $0,1,N$ cavity modes; the third with $1,0,N$ cavity modes; the fourth with $0,2,N$; the fifth with $1,1,N$; and the sixth

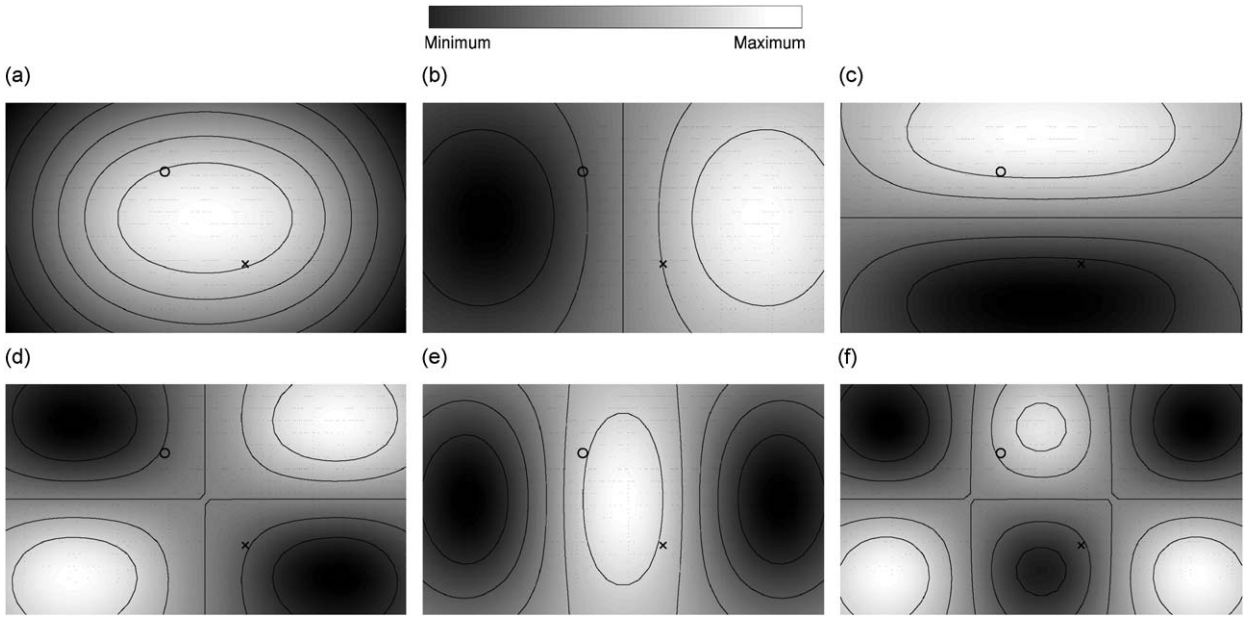

Fig. 4. Orthogonal sound pressure shapes in the near vicinity of a planar radiator radiating into the cavity: orthogonal radiation pattern (a) one, (b) two, (c) three, (d) four, (e) five, (f) six.

$1, 2, N$. One of the implications of this selective coupling is that as the number of cavity modes increases, if the indices of the cavity modes do not fall into any of these sets more and more orthogonal radiation patterns will be needed to be measured and then minimized—to achieve a broadband reduction of the global error.

3.2. Attenuation of the global error

The aim of the control simulations is to test what level of global attenuation occurs when the resolved multipole radiation patterns are minimized, and compare this to the level of global attenuation that is maximally possible with the given control source placement. The modelling technique is the standard open-loop approach, where the quadratic error criterion is minimized analytically; a result that is *independent* of the precise control approach (i.e. feedforward or feedback, etc.) that is used in practice. An overview of the technique, applied to controlling acoustic radiation (pressure) from a simply supported rectangular panel can be found in Ref. [34].

Consider now the case where an active control system is built on the orthogonal radiation patterns, shown in Fig. 4, as error signals. The implementation will use vibration sensors placed at the location of each virtual monopoles used in the decomposition, these structural signals are then filtered to estimate the orthogonal radiation patterns forming the error signals which are then minimized. The general physical and mathematical approach are illustrated in Fig 2.

In the control simulation a primary disturbance is located at (0.117 m, 0.272 m) (x, y), relative to the bottom left corner of the panel. A control source is located at (0.273 m, 0.408 m). Two sensing strategies will be investigated in simulation: one that uses measurements obtained in the vibration domain, the other from the acoustic domain. In each case 32 sensors will be used, matching the number of virtual monopoles used in the decomposition process of the global error. The sensors are placed at the locations of the virtual monopoles. In this case the modal filtering weights to derive the six orthogonal contributors emulating from the panel into the cavity are defined in Eqs. (29) and (30). Illustrated in Fig. 5 are the normalized weights shown for each sensor location.

3.2.1. Vibration sensing

While the sensing system design approach developed here is very much acoustic-centric, with a set of orthogonal acoustic functions describing the global error, it is still important to be able to implement the strategy with vibration sensors (as they do have some positive points for global acoustic problems). Such structural sensing systems are an integral part of much current smart structure research to which the approach developed here is amendable.

Fig. 6 shows the reduction in the global error, acoustic potential energy, when the first, the first four and all six orthogonal radiation patterns from the panel to the acoustic potential energy are controlled. For comparison is the maximum achievable attenuation for the given control arrangement. The result in Fig. 6 uses multipole radiation patterns as defined in Eq. (11) evaluated at a single frequency, 1 Hz. With this single (fixed frequency) result for $\psi(\mathbf{r})$ the coupling matrix $\boldsymbol{\beta}_{i,j}$ has been calculated (Eq. (19)). This single (fixed frequency) result of $\boldsymbol{\beta}_{i,j}$ has then been assumed constant for the

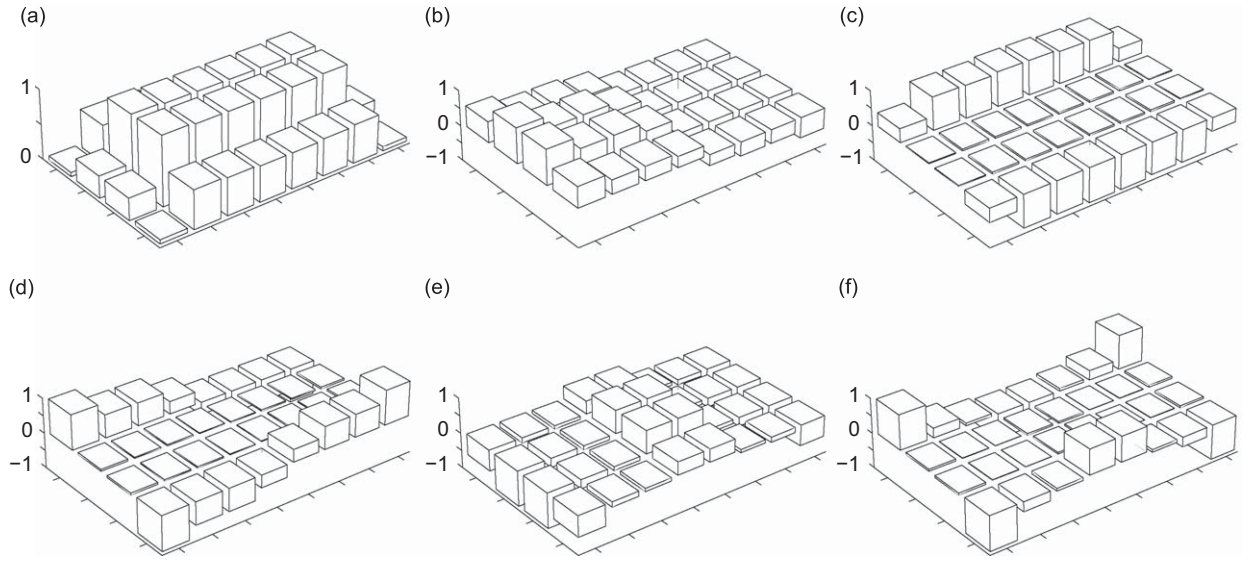

Fig. 5. The normalized modal filter weights for the sensors places at the virtual monopole locations: weight set (a) one, (b) two, (c) three, (d) four, (e) five, (f) six.

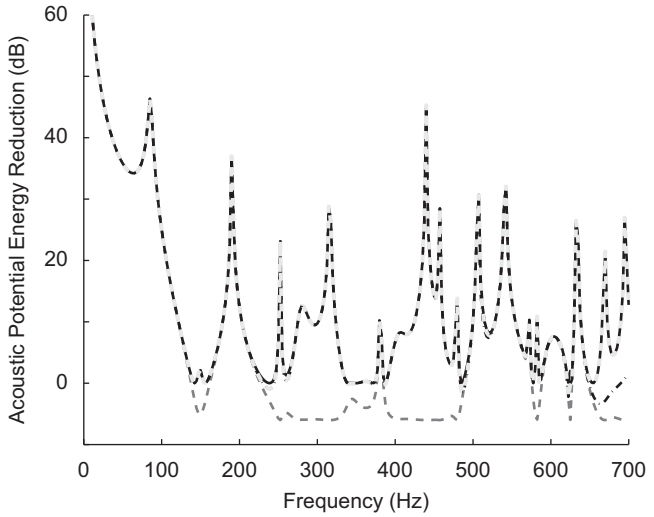

Fig. 6. Attenuation of the global error, acoustic potential energy when minimizing the first orthogonal radiation pattern — — —, the first four -·-·-·-, all six — — —, and the maximum achievable ———.

calculation of $\mathbf{A}$ (Eq. (25)), from which $\mathbf{Q}^{-1}$ follows. In the simulation $\mathbf{Q}^{-1}$ has been calculated at 10 Hz, and assumed constant over the entire frequency range (0–700 Hz). There is some flexibility with regards to which frequency to evaluate $\mathbf{Q}^{-1}$ because over the considered frequency range the values are relatively constant. Here different frequencies at which to evaluate $\boldsymbol{\beta}_{i,j}$ and $\mathbf{Q}^{-1}$ have been chosen just to show the technique works when $\mathbf{Q}^{-1}$ is evaluated at a frequency different to that where $\boldsymbol{\beta}_{i,j}$ is evaluated (the same results in attenuation of the global error result when $\mathbf{Q}^{-1}$ is evaluated at 1 Hz, however, the frequency at which to evaluate $\boldsymbol{\beta}_{i,j}$ is going to be restricted by the minimum sphere issue discussed earlier). Finally the resulting quantities in $\boldsymbol{a}_{\text{ortho}}$ (Eq. (30)) are weighted by the frequency dependent weights in $\boldsymbol{\Lambda}$.

As would be expected, attenuating the first orthogonal radiation pattern delivers excellent control at the cavity mode frequencies, which the first radiation pattern couples well too. Observe that when the first four orthogonal radiation patterns are minimized the maximum possible attenuation is achieved over the entire frequency range at all frequencies except around the two highest cavity modes where the fifth and six orthogonal radiation patterns are the dominant contributors to the global error. Fig. 6 clearly demonstrates that the combined assumptions (that, $\psi(\boldsymbol{r})$ is evaluated just in front of the panel (rather than on it); that the evaluation is at a single frequency, for a broadband problem; that the eigenvectors $\mathbf{Q}^{-1}$ are fixed over the entire frequency range) do not influence the maximum achievable attenuation.

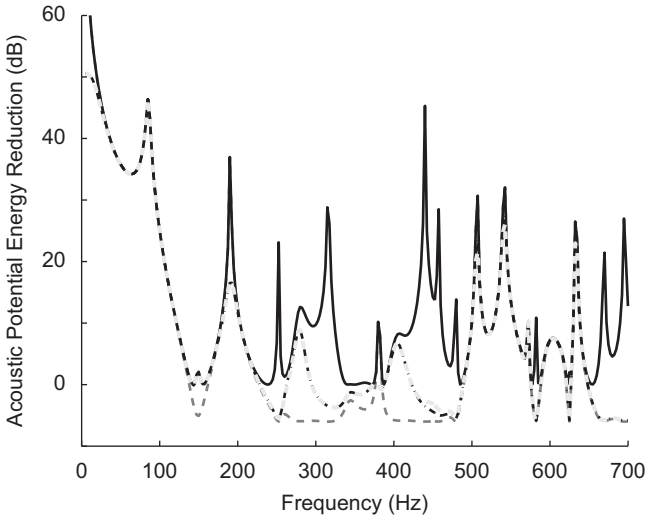

Fig. 7. Attenuation of the global error, acoustic potential energy when minimizing the first orthogonal radiation pattern – – – –, the first four –·–·–·–, all six – – – –, and the maximum achievable ——— (eigenvalue weights are fixed at 100 Hz values).

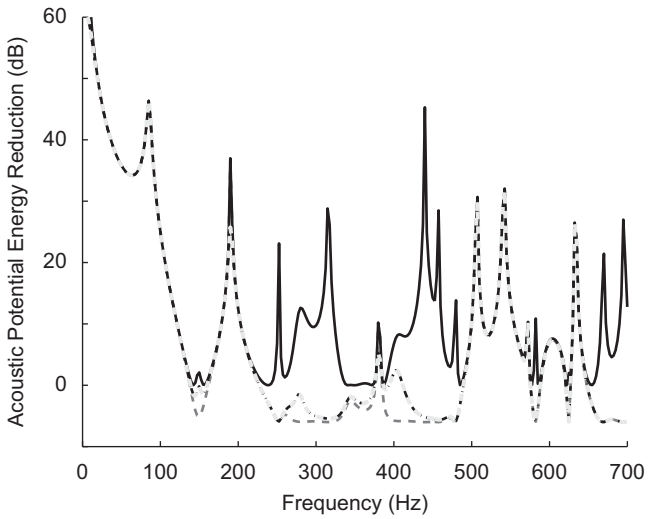

Fig. 8. Attenuation of the global error, acoustic potential energy when minimizing the first orthogonal radiation pattern – – – –, the first four –·–·–·–, all six – – – –, and the maximum achievable ——— (eigenvalue weights are fixed at 200 Hz values).

Therefore each assumption is shown to be practically workable. In summary, what has been demonstrated is the minimization of a generalized set of orthogonal error functions which are applicable to *any* type of noise source radiating into an acoustic cavity is capable of achieving the maximum theoretical possible for a given control arrangement, as long as the assumptions made in the development are also valid. Consequently, in terms of the reduction of the global error, the decomposition technique offers no obstacles to achieve the best possible global attenuation.

Having seen that the approach of minimizing the orthogonal radiation pattern amplitudes, calculated using the eigenvectors of the error weighting matrix $\mathbf{A}$ that are strictly only correct for a single frequency (as could be measured by something like a shaped sensor), weighted by the eigenvalue ($\mathbf{\Lambda}$, illustrated in Fig. 3) evaluated at each frequency is theoretically capable of producing the maximum achievable for the given set up; the final question to address is it a practical approach? While it is straightforward to implement in simulation the frequency dependent eigenvalue weightings ($\mathbf{\Lambda}$), in practice this means the construction of a frequency dependent filter with the shape corresponding to that in Fig. 3. To answer this question consider the case where the control strategy uses fixed eigenvalue weightings (evaluated at a single frequency) over the entire frequency range 5–700 Hz. Illustrated in Figs. 7–9 is the attenuation achieved when one, four and all six of the orthogonal radiation patterns are minimized. The figures follow the exact procedure used for Fig. 6, except here the eigenvalue weightings ($\mathbf{\Lambda}$) are fixed at 100, 200 and 300 Hz, respectively. Observe that the achieved

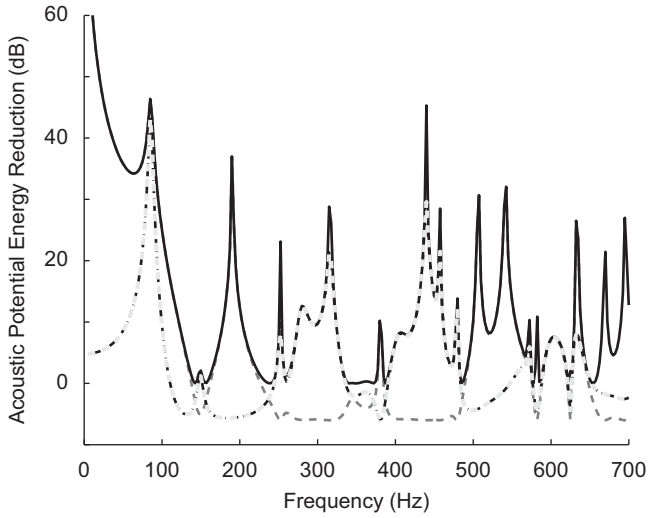

Fig. 9. Attenuation of the global error, acoustic potential energy when minimizing the first orthogonal radiation pattern – – –, the first four –·–·–·–, all six – – – –, and the maximum achievable ——— (eigenvalue weights are fixed at 300 Hz values).

attenuation of the global error is far less impressive than in Fig. 6, where the eigenvalue weights were calculated at each discrete frequency. Overall Figs. 7–9 show that the maximum level of attenuation is achieved at or near the 'perfect' frequency, where the eigenvalues are evaluated. However, at other frequencies attenuation close to the maximum achievable (or that achieved in Fig. 6 for a small number of orthogonal radiation patterns) will only be achieved where the relative ratios of the values in $\mathbf{\Lambda}$ at the 'perfect' frequency are similar to those at other frequencies. The results in Figs. 7–9 indicate the importance of obtaining a set of errors which *accurately* reflect the global quantity to be minimized. In this example the problem is that the vibration sensors on the panel do not measure the acoustic modes accurately or even at all. Observe in Figs. 7–9, the 18th and 19th cavity modes are never controlled as the sensing system never measures any spectral peaks at the corresponding frequencies contributing to the global error. The simulation shows that in the vibration-centric sensing approach here, what is measured is essentially just the panel vibration modes, hence for system spectral peaks controlled by the cavity to be present in the amplitudes of the orthogonal contributors (which are minimized) these signals must be weighted by eigenvalue amplitudes ($\mathbf{\Lambda}$) to effectively include the resonance frequencies controlled by the cavity in the error. The reason that the acoustic controlled modes are not measured well on the structure is essentially due to the weak coupling within the system, or in loose terms, the cavity modes do not have enough authority over the panel to be present in measurements taken on the panel. For control of sound transmission into coupled cavities, sensing vibration to obtain an estimate of acoustic potential energy will then be a practical concern for any decomposition method of the global error.

In terms of a practical active noise control system the main issue for the decomposition here is the ease to which a filter with frequency characteristics dictated by the singular values associated with the eigenvalues plotted in Fig. 3 can be constructed. Essentially this problem reduces to constructing a set of filters that will mirror the response spectrum of a specific set of acoustic modes. While this is possible, it is not as straightforward as the construction of what are essentially high-pass filters for the control of acoustic power in the free field, which based on similar global, generalized functions have been successfully completed in experiments [23,25]. Furthermore, the problem becomes more complicated as modal density increases, requiring the measurement and control of evermore orthogonal radiation patterns. Therefore while the use of structural velocity measurements as error signals in active control systems targeting attenuation of sound transmission into coupled enclosures using vibration control sources is feasible, practical implementation needs to be assessed on a per-problem basis. The critical factors determining practical implementation are: the frequency range of interest; and modal density of the enclosure.

Based on this considerable drawback to practical implementation, acoustic sensing of the orthogonal radiation patterns will be investigated.

3.2.2. *Acoustic sensing*

Instead of vibration sensors on the panel measuring the virtual monopole amplitudes, in this section microphones adjacent the vibrating surface are used to measure the virtual monopole amplitudes. The physical arrangement and the mathematical procedure are similar to that illustrated in Fig. 2. The beauty of the generalized sensing technique presented here is that the modal filter weights are general; not only in their application to any *type* noise source but also the *domain* to which the virtual monopole amplitudes are being measured. This simulation will illustrate this point.

The locations of the 32 microphones are positioned at the location of the virtual monopoles over the x-y plane at 0.1 m from the panel (where $\psi(\boldsymbol{r})$ was evaluated for $\boldsymbol{\beta}_{ij}$ and thus the modal filtering weights), thus they will measure the virtual monopole amplitudes directly, thereby simplifying the sensing procedure to that described in Eq. (29). By using such placement the outputs will contain both the spectral peaks controlled by the panel and also the spectral peaks controlled by the acoustic cavity. As will be shown the presence of spectral peaks controlled by each domain (structural and acoustic) in the error signal will make a significant difference in a broadband practical system.

As a consequence of the decomposition technique being generalized, exactly the same modal filtering weights are used as in the previous section to resolve the amplitudes orthogonal radiation patterns. As a starting point, like the previous section, the frequency variation of the eigenvalues is included in the calculation. The location of the disturbance and control point forces on the panel remain the same as in the previous section. Illustrated in Fig. 10 is the attenuation achieved when the first; first four; and all six multipole patterns (orthogonal contributors to acoustic potential energy within the cavity) are minimized. The maximum achievable attenuation for the given source arrangement is plotted for assessment of the techniques viability. Observe the similarity of the results with that in Fig. 6 where vibration sensors were used to obtain the amplitudes of the orthogonal radiation patterns.

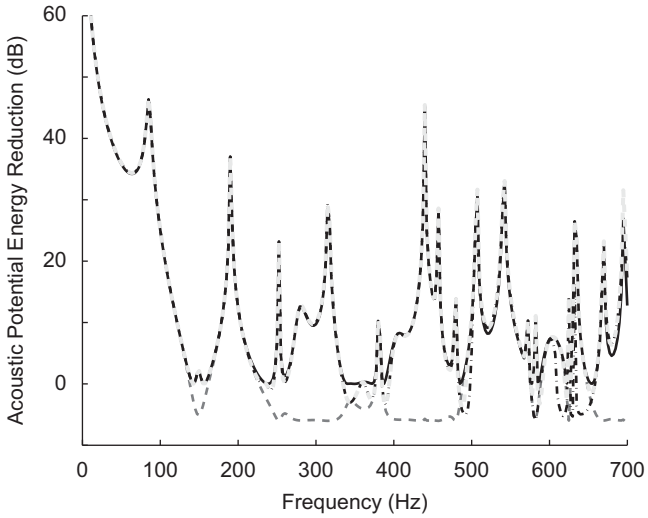

Fig. 10. Attenuation of the global error, acoustic potential energy when minimizing the first orthogonal radiation pattern – – – –, the first four –·–·–·–, all six – – – –, and the maximum achievable ————; acoustic sensing.

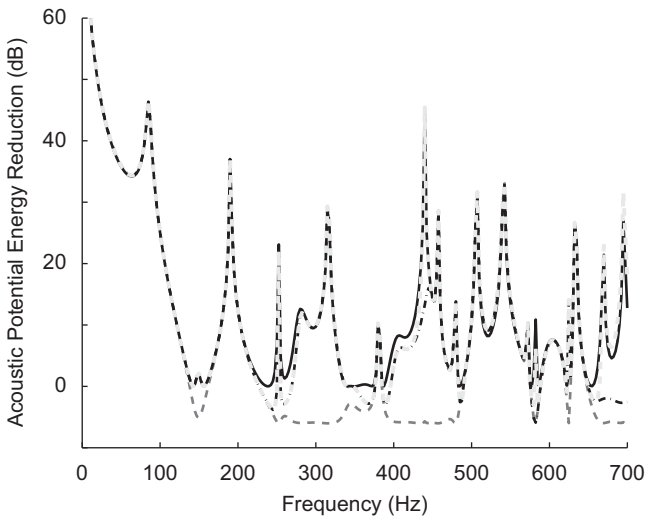

Fig. 11. Attenuation of the global error, acoustic potential energy when minimizing the first orthogonal radiation pattern – – – –, the first four –·–·–·–, all six – – – –, and the maximum achievable ———— (eigenvalue weights are fixed at 100 Hz values); acoustic sensing.

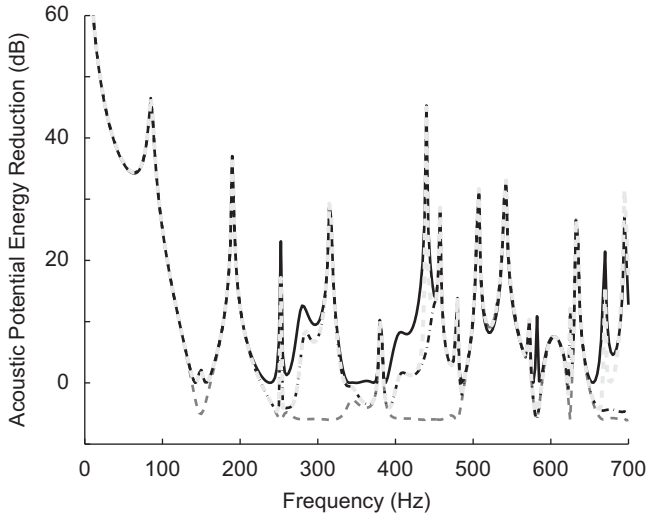

Fig. 12. Attenuation of the global error, acoustic potential energy when minimizing the first orthogonal radiation pattern – – – –, the first four –·–·–·–, all six – – – –, and the maximum achievable ——— (eigenvalue weights are fixed at 200 Hz values); acoustic sensing.

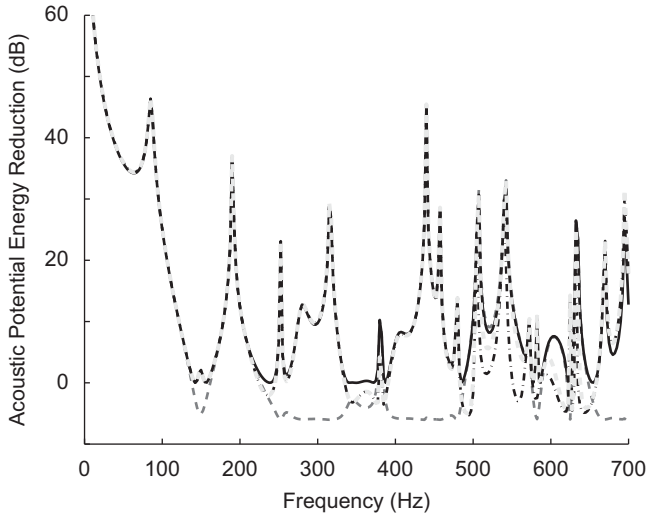

Fig. 13. Attenuation of the global error, acoustic potential energy when minimizing the first orthogonal radiation pattern – – – –, the first four –·–·–·–, all six – – – –, and the maximum achievable ——— (eigenvalue weights are fixed at 300 Hz values); acoustic sensing.

It was illustrated in the previous section that when the frequency dependent weighting factors, $\mathbf{\Lambda}$, are ignored the performance of the system is significantly reduced, limiting the application of structural based sensing systems to practical situations with a low modal density or a narrow frequency range of interest. Consider now the case where the frequency dependent variation of $\mathbf{\Lambda}$, used in the sensing procedure illustrated in Fig. 2, is ignored for the acoustic sensing case. Illustrated in Figs. 11–13 is the attenuation achieved when the first; first four; and all six multipole patterns are controlled. Observe that while each figure indicates some loss of performance in comparison to Fig. 10, the reduction would not be in the order to render the approach impractical, in the situation where a broad frequency range is considered and the target enclosure is modally dense. Such an outcome is a significant improvement over structural sensing and an important development for practical implementation as the best possible attenuation can be expected when the generalized radiation patterns are measured in the acoustic domain. The generalizing of the global error construction and the resulting sensing approach simplifies greatly the implementation of active control systems for noise radiation into cavities by overcoming the shortfalls of structural-centric approaches and thus opening application to practical situations beyond the laboratory.

There are several factors which contribute to the good attenuation in the global error when the frequency dependency of the eigenvalues weights, $\mathbf{\Lambda}$, is ignored when acoustic sensors are used. Two factors appear most important. Firstly the sensors measure acoustic quantities, which are *directly* related to the acoustic global error (as opposed to structural sensors

which are only *directly* related to vibration quantities). Secondly is the location of the sensors. As an acoustic quantity is measured within the cavity, the acoustic characteristics of the cavity will be present in sensor outputs, that is the spectral peaks controlled by the cavity will already be present in the amplitudes of the orthogonal radiation patterns (Eq. (29)). Consider also that due to the close proximity of the acoustic sensors to the panel, spectral peaks controlled by the structural modes are also present. The end result is that the multipole amplitudes (the orthogonal error signals) contain spectral peaks associated with all system resonances—structural and acoustic. As shown by the simulation results, in the acoustic sensing case the need for frequency dependent weighting of the multipole amplitudes is significantly reduced.

4. Conclusions

A novel generalized approach to the sensing of functions, which contribute orthogonally to the global error (potential energy), within an enclosure has been presented. The developed orthogonal functions are generalized, as they are fundamentally acoustic based and thus not constrained to being applied to structural sources or defined by structural measurements. Therefore application can be made to any noise source, facilitating wide practical implementation of the technique. The presented approach makes a significant improvement over previous work, which has taken a vibration-centric approach working with structural modes and postulating structural measurements. The requirement of detailed structural knowledge inherent in such approaches has limited the hope of moving beyond small-scale laboratory implementations to more practical problems.

The development of the orthogonal multipoles for cavity noise is built on fundamental acoustic radiation patterns, generated from an array of virtual monopoles whose phases are defined by the Hadamard matrix. It was shown that the most efficient radiator for a planar radiator transferring energy into the enclosure is monopole like. The second and third were shown to be dipole like and the fourth a quadrupole like. A strength of the decomposition strategy is that in the use of these fundamental acoustic shapes, the radiation from any source into the enclosure can be divided up into a small set of orthogonal contributors, giving the designer a target for a quantity to measure and control.

Simulations were completed to illustrate the validity of the novel approach by illustrating that a controller minimizing the generalized orthogonal functions will achieve the maximum possible attenuation of the global error. The simulation target was the case where a vibrating panel is radiating into an enclosure. The control approach sought to minimize the global error within the cavity, based on minimizing the small set of multipole amplitudes, filtered from a larger number of sensors. Attenuation of the global error using structural sensors and acoustic sensors was presented. The results indicated that using both structural and acoustic sensors provided an error signal, which enabled the maximum level of global error attenuation to be achieved. That the generalized decomposition method provides no obstacle to the active control system achieving the maximum possible attenuation of the global error proved that the assumptions made in the development are indeed workable. Furthermore as the decomposition is general, the technique is capable of achieving maximum attenuation in any given physical set-up provided that the same assumptions made in the development (weak coupling, etc.) are also valid in the practical case being considered.

Practical aspects of the active control implementation were also considered in the simulations. It was shown that ultimately using vibration based sensors to measure the multipole amplitudes will only be a practical solution in particular cases. The limiting factor for practical implementation of a structural based sensing approach is the construction of filters that will match the response spectrum of a specific set of acoustic modes. While this is possible, it is not straightforward, particularly as modal density and the frequency range of interest increases.

However, an active noise control system built on acoustic sensors and structural actuators showed that even when the frequency dependence of the eigenvalues of the weighting matrix are ignored, the level of attenuation is still relatively close to the maximum theoretically possible. The reason for the difference is that the structural measurements alone do not contain the spectral peaks controlled by the cavity (on the whole). As not all system spectral peaks are present in the error estimate, control effectiveness is reduced. In the case of acoustic sensors placed in the close vicinity of the panel, the filtered multipole amplitudes will contain all system spectral peaks (both structural and acoustic controlled peaks), therefore the frequency dependent weights defined by the eigenvalues are not as important and control of the global error is not influenced as much over a wide frequency range.

Overall the results indicated that for an enclosed structural–acoustic system where the goal is to reduce a global acoustic property, acoustic sensors yield the optimal and more practical solution.

References

[1] R.H. Lyon, Noise reduction of rectangular enclosures with one flexible wall, *Journal of the Acoustical Society of America* 35 (11) (1963) 1791–1797.
[2] A.J. Pretlove, Free vibrations of a rectangular panel backed by a closed rectangular cavity, *Journal of Sound and Vibration* 2 (3) (1965) 197–209.
[3] A.J. Pretlove, Forced vibrations of a rectangular panel backed by a closed rectangular cavity, *Journal of Sound and Vibration* 3 (3) (1966) 252–261.
[4] L.D. Pope, On the transmission of sound through finite closed shells: statistical energy analysis, modal coupling, and non-resonant transmission, *Journal of the Acoustical Society of America* 50 (3) (1971) 1004–1018.
[5] R.W. Guy, M.C. Bhattacharya, The transmission of sound through a cavity-backed finite plate, *Journal of Sound and Vibration* 27 (1973) 207–223.
[6] P.A. Nelson, A.R.D. Curtis, S.J. Elliott, A.J. Bullmore, The active minimization of harmonic enclosed sound fields, part I: theory, *Journal of Sound and Vibration* 117 (1) (1987) 1–13.

[7] A.J. Bullmore, P.A. Nelson, A.R.D. Curtis, S.J. Elliott, The active minimisation of harmonic enclosed sound fields, part II: a computer simulation, *Journal of Sound and Vibration* 117 (1) (1987) 15–33.
[8] C.R. Fuller, J.D. Jones, Experiments on reduction of propeller induced interior noise by active control of cylinder vibration, *Journal of Sound and Vibration* 112 (2) (1987) 389–395.
[9] S.J. Elliott, A.R.D. Curtis, A.J. Bullmore, P.A. Nelson, The active minimisation of harmonic enclosed sound fields, part III: experimental verification, *Journal of Sound and Vibration* 117 (1) (1987) 35–58.
[10] J.D. Jones, C.R. Fuller, Active control of sound fields in elastic cylinders by multicontrol forces, *AIAA Journal* 27 (7) (1989) 845–852.
[11] C.R. Fuller, S.D. Snyder, C.H. Hansen, R.J. Silcox, Active control of interior noise in model aircraft fuselages using piezoceramic actuators, *AIAA Journal* 30 (11) (1992) 2613–2617.
[12] J. Pan, C.H. Hansen, D.A. Bies, Active control of noise transmission through a panel into a cavity: I. Analytical study, *Journal of the Acoustical Society of America* 87 (5) (1990) 2098–2108.
[13] J. Pan, C.H. Hansen, Active control of noise transmission through a panel cavity: II. Experimental study, *Journal of the Acoustical Society of America* 90 (3) (1991) 1488–1492.
[14] S.D. Snyder, N. Tanaka, On feedforward active control of sound and vibration using vibration error signals, *Journal of the Acoustical Society of America* 94 (4) (1993) 2181–2193.
[15] S.D. Snyder, C.H. Hansen, The design of systems to actively control periodic sound transmission into enclosed spaces, part 1: analytical models, *Journal of Sound and Vibration* 170 (4) (1994) 433–449.
[16] S.D. Snyder, C.H. Hansen, The design of systems to actively control periodic sound transmission into enclosed spaces, part 2: mechanisms and trends, *Journal of Sound and Vibration* 170 (4) (1994) 451–472.
[17] S.M. Kim, M.J. Brennan, Active control of harmonic sound transmission into an acoustic enclosure using both structural and acoustic actuators, *Journal of the Acoustical Society of America* 107 (5) (2000) 2523–2534.
[18] N. Tanaka, K. Kobayashi, Cluster control of acoustic potential energy in a structural/acoustic cavity, *Journal of the Acoustical Society of America* 119 (5) (2006) 2758–2771.
[19] T. Kaizuka, N. Tanaka, Radiation clusters and the active control of sound transmission through symmetric structures into free space, *Journal of Sound and Vibration* 311 (1–2) (2008) 160–183.
[20] B.S. Cazzolato, C.H. Hansen, Active control of sound transmission using structural error sensing, *Journal of the Acoustical Society of America* 104 (5) (1998) 2878–2889.
[21] S.J. Elliott, M.E. Johnson, Radiation modes and the active control of sound power, *Journal of the Acoustical Society of America* 94 (4) (1993) 2194–2204.
[22] S.G. Hill, S. D Snyder, B.S. Cazzolato, N. Tanaka, R. Fukuda, A generalised approach to modal filtering for active noise control, part II: acoustic sensing, *IEEE Sensors* 2 (6) (2002) 590–596.
[23] S.D. Snyder, S.G. Hill, N.C. Burgan, N. Tanaka, B.S. Cazzalato, Acoustic-centric modal filter design for active noise control, *Control Engineering Practice* 12 (8) (2004) 1055–1064.
[24] S.G. Hill, S.D. Snyder, Acoustic based modal filtering of orthogonal radiating functions for active noise control: part I theory and simulation, *Mechanical Systems and Signal Processing* 21 (4) (2007) 1815–1838.
[25] S.G. Hill, N. Tanaka, S.D. Snyder, Acoustic based modal filtering of orthogonal radiating functions for active noise control: part II implementation, *Mechanical Systems and Signal Processing* 21 (5) (2007) 1937–1952.
[26] S.G. Hill, S.D. Snyder, N. Tanaka, Acoustic based modal filtering experiments, *Applied Acoustics* 68 (11–12) (2007) 1400–1426.
[27] S.G. Hill, S.D. Snyder, N. Tanaka, Acoustic based sensing of orthogonal radiating functions for three-dimensional noise sources: background and experiments, *Journal of Sound and Vibration* 318 (4–5) (2008) 1050–1076.
[28] H.F. Harmuth, *Transmission of Information by Orthogonal Functions*, second ed., Springer, Berlin, 1972.
[29] R.J. Pinnington, D.C.R. Pearce, Multipole expansion of the vibration transmission between a source and receiver, *Journal of Sound and Vibration* 142 (3) (1990) 461–479.
[30] K.A. Cunefare, The minimum multimodal radiation efficiency of baffled finite beams, *Journal of the Acoustical Society of America* 90 (5) (1991) 2521–2529.
[31] N.C. Burgan, S.D. Snyder, N. Tanaka, A.C. Zander, A generalised approach to modal filtering for active noise control, part I: vibration sensing, *IEEE Sensors Journal* 2 (6) (2002) 577–589.
[32] S.F. Wu, On reconstruction of acoustic pressure fields using the Helmholtz equation least squares method, *Journal of the Acoustical Society of America* 107 (5) (2000) 2511–2522.
[33] C. Yu, Z. Zhou, M. Zhuang, An acoustic intensity-based method for reconstruction of radiated fields, *Journal of the Acoustical Society of America* 123 (4) (2008) 1892–1901.
[34] C.H. Hansen, S.D. Snyder, *Active Control of Noise and Vibration*, E & FN Spon, London, 1997.